# First-principles calculation of the band offset at $BaO/BaTiO_3$ and $SrO/SrTiO_3$ interfaces.

Javier Junquera,[1] Magali Zimmer,[1] Pablo Ordejón,[2] and Philippe Ghosez[1]

[1] *Département de Physique, Université de Liège, Bâtiment B-5, B-4000 Sart-Tilman, Belgium*
[2] *Institut de Ciència de Materials de Barcelona, CSIC, Campus de la UAB, Bellaterra, 08193 Barcelona, Spain*

(Dated: February 6, 2008)

We report first-principles density-functional pseudopotential calculations on the atomic structures, electronic properties, and band offsets of $BaO/BaTiO_3$ and $SrO/SrTiO_3$ nanosized heterojunctions grown on top of a silicon substrate. The density of states at the junction does not reveal any electronic induced interface states. A dominant perovskite character is found at the interface layer. The tunability of the band offset with the strain conditions imposed by the substrate is studied. Using previously reported theoretical data available for Si/SrO, Si/BaO and $BaTiO_3/SrRuO_3$ interfaces we extrapolate a value for the band alignments along the whole gate stacks of technological interest: $Si/SrO/SrTiO_3$ and $Si/BaO/BaTiO_3/SrRuO_3$ heterostructures.

PACS numbers: 73.20.At, 73.40.Qv, 73.30+y

## I. INTRODUCTION

The search for alternative gate dielectric materials to replace silica ($SiO_2$) in microelectronic devices is one of the grand challenges that the materials science community and the Si-based semiconductor industry are facing at the current time [1]. The rapid scaling of the physical gate lengths of Metal-Oxide-Semiconductor Field-Effect-Transistors (MOSFET) requires a concomitant rapid reduction of the gate dielectric thickness in order to preserve a high gate oxide capacitance. This can no more be accomplished by lowering the size of the $SiO_2$ layer because, together with problems in the thickness control, the leakage current would become inacceptably high. Indeed, the leakage current from the channel to the gate is due to the direct tunneling of carriers and increases exponentially with the decrease of both the thickness of the gate dielectric and the height of the electrostatic barrier for the electrons through the gate stack. The current roadmap projection (assessed by the the International Technology Roadmap for Semiconductors, ITRS [2]) imposes the choice of an alternative gate dielectric with a good capacitance for a thick-enough layer and its full implementation into the production line by 2005.

The properties that the new dielectric should meet are well established and have been reviewed recently by Wilk and Wallace[3]. They can be divided into *fundamental material properties*, and *device processing and performance properties*. Amongst the material properties, we can enumerate (*i*) a higher dielectric constant than amorphous silica ($\kappa_{SiO_2} = 3.9$) in order to increase the capacitance without decreasing the thickness, (*ii*) large band gaps and band offsets with Si to prevent tunneling currents, (*iii*) a good thermodynamic stability in contact with the Si substrate, (*iv*) a good quality of the interface with the Si channel, which means a small number of electrical defects and a low midgap interface state density, and (*v*) film morphology avoiding the formation of polycristalline films and grain boundaries. Amongst the device properties, we can cite (*vi*) a good compatibility with metallic gate electrodes, (*vii*) a compatiblity with the deposition mechanism during the fabrication process, (*viii*) reliability.

Many materials satisfy some subset of the previous criteria, but the identification of a dielectric that addresses *simultaneously* all of the requirements is a real challenge. Investigations on oxides like $Al_2O_3$, $ZrO_2$, $HfO_2$, $Ta_2O_5$, $Y_2O_3$, $Gd_2O_3$, and $TiO_2$, have thrown encouraging results in the last few years[4]. Amongst the most promising candidates, $ABO_3$ perovskite oxides (where A stands for Ba or Sr and B stands for Ti) appear in good position.

The $ABO_3$ compounds have a dielectric constant above 300, one order of magnitude higher than the other candidates. Although they are thermodynamically unstable in direct contact with Si (they react to form titanium silicide and alkaline-earth silicate[4,5]), they can be grown in perfect registry with the Si substrate by means of Molecular Beam Epitaxy (MBE) when including a silicon-compatible buffer layer. On one hand, this layer must be sufficiently thick to ensure the physical separation between the substrate and the perovskite. On the other hand, it must remain thin enough to keep the benefit of the high dielectric constant of the $ABO_3$ compound (the capacitance of the lower-$\kappa$ buffer layer being in series with that of the perovskite).

In the McKee-Walker process[6,7,8], the buffer consists in few atomic layers of AO alkaline-earth oxide that can eventually be alloyed during the growth in order to accomodate the lattice mismatch with Si. The growth of AO on Si includes the presence, at the interface, of a (sub)monolayer of $ASi_2$ silicide so that the final structure corresponds to the sequence $Si/ASi_2/AO/ABO_3$. The epitaxy is such that $ABO_3\,(001) \parallel AO\,(001) \parallel Si\,(001)$, and $ABO_3\,\langle 110\rangle \parallel AO\,\langle 100\rangle \parallel Si\,\langle 100\rangle$, i. e. the $ABO_3$ atomic planes are rotated 45° around the (001) AO direction [9]. The epitaxial crystalline growth at the oxide/semiconductor interface avoids the formation of de-

fects and ensures the continuity of the dielectric displacement [7]. MBE techniques allow the control of the growing sequence at the submonolayer level preventing grain-boundaries and providing a good quality interface and extremly smooth surface morphology.

First attempts to make MOSFETs including perovskite oxides have been reported recently. Using a 110 Å-thick $SrTiO_3$ layer as the gate dielectric, Eisenbeiser *et al* [10] have fabricated a transistor that behaves comparably to a 8 Å-thick $SiO_2$/Si MOSFET. The improvement in transistor performance was very satisfactory, and the leakage currents was two order of magnitudes smaller than in a similar $SiO_2$-based device.

As it was pointed out before, the barrier height of the dielectric with respect to the Si substrate should be large enough to minimize carrier injection into the conduction band states. A large value of the Conduction Band Offset, CBO, between Si and the gate dielectric is required, and typically materials with CBO smaller than 1.0 eV are rejected for further applications. Robertson and Chen [11], aligning the Charge Neutrality Levels (CNL)[12] of both semiconductors, have estimated the CBO for a Si/$SrTiO_3$ interface to -0.14 eV ($SrTiO_3$ below, that is no barrier at all for the electrons) in very good agreement with experimental results[13]. This prevents, in principle, the use of the titanate as the gate dielectric in electronic devices. However, the presence of the buffer alkaline-earth oxide in the heterostructure was missing in their approach. In this paper, we will show that in addition to providing a physical separation between Si and the perovskite, the presence of the alkaline-earth oxide also allows to monitor efficiently the band offset.

We report a study of the properties of BaO/$BaTiO_3$ (from now on, we will refer to this heterostructure as the Ba-interface), and SrO/$SrTiO_3$ (Sr-interface) structures from first-principles. The method on which the simulations are based is described in Section II. In Section III, we discuss the details of the atomic structure at the interfaces. The electronic structure is presented in Sections IV, where we analyze the density of states at the junctions. In Section V we study the band-offset at the interface. Finally, in Section VI, an estimate of the band alignment of the whole whole Si/SrO/$SrTiO_3$/Pt and Si/BaO/$BaTiO_3$/$SrRuO_3$ structures will be given.

## II. TECHNICALITIES

Our calculations have been performed within Density Functional Theory (DFT) [14] and the Local Density Approximation (LDA) [15]. We used a Numerical Atomic Orbital (NAO) method, as it is implemented in the SIESTA code [16,17,18]. The exchange-correlation functional was approximated using the Perdew and Zunger [19] parametrization of Ceperley-Alder data[20].

Core electrons were replaced by *ab-initio* norm-conserving fully-separable[21] Troullier-Martin[22] pseudopotentials. Due to the large overlap between the semicore and valence states, the $3s$ and $3p$ electrons of Ti, $4s$ and $4p$ electrons of Sr, and $5s$ and $5p$ electrons of Ba were explicitly included in the calculation. Ti, Sr and Ba pseudopotentials were generated scalar-relativistically. The reference configuration and cutoff radii for all the atoms we used are shown in Table-I.

The one-electron Kohn-Sham eigenstates were expanded in a basis of strictly-localized [23] Numerical Atomic Orbitals [24]. Basis functions were obtained by finding the eigenfunctions of the isolated atoms confined within the new soft-confinement spherical potential proposed in Ref. 25. We used single-$\zeta$ basis set for the semicore states of Ti, Sr and Ba, and double-$\zeta$ plus polarization for the valence states of all the atoms. For Sr (respectively Ba) an extra shell of $4d$ (respectively $5d$) orbitals was added. All the parameters that define the shape and the range of the basis functions for Ba, Ti and O were obtained by a variational optimization in cubic bulk $BaTiO_3$, following the procedure described in Ref. 25. For Sr, another optimization was performed in bulk $SrTiO_3$, frozen in the atomic orbitals of Ti and O to these previously optimized in $BaTiO_3$ [26].

The electronic density, Hartree and exchange-correlation potentials, as well as the corresponding matrix elements between the basis orbitals, were calculated in an uniform real-space grid [16]. An equivalent plane wave cutoff of 200 Ry was used to represent the charge density. Once self-consistency was reached, the grid was refined (reducing the distance between grid points by half) to compute the total energy, atomic forces and stress tensor.

The integrals in reciprocal space were well converged, using in all the cases a sampling in $\vec{k}$ of the same quality as the $(6 \times 6 \times 6)$ Monkhorst-Pack [27] mesh in bulk $BaTiO_3$. The equivalent cutoff-length [28] for this sampling, 13 Å, was the one employed in all simulations. This represents a large number of $\vec{k}$-points thought that all the materials involved in the heterojunctions are insulators. However it has been proved that this fineness is mandatory while dealing with perovskites [29].

Test of the performance of the SIESTA method on perovskites were done in bulk $BaTiO_3$[30]. Lattice constants, ferroelectric distorsions, Born effective charges, and phonon dispersion curves are in very good agreement with plane waves [29,31,32,33] and full potential LAPW calculations [34].

## III. ATOMIC STRUCTURE AT THE INTERFACE

In Table II we report the experimental and calculated lattice parameters of the different materials involved in our heterostructures, together with the lattice mismatch with respect to the Si substrate. The misfit is defined as $f = 100 \times (a - a_{Si}) / a_{Si}$, where $a$ and $a_{Si}$ are, respectively, the lattice constant of the epilayer and Si. The value of $f$ is positive when the epilayer is compressed

TABLE I: Reference configuration and cutoff radii (in bohr) of the pseudopotentials used in our study. Because of the inclusion of the semi-core states in valence, and within the Troullier-Martin scheme, Ba, Ti, and Sr pseudopotentials must be generated for ionic configurations (ionic charge +2). However, these are more suitable than the neutral ones, given the oxidation numbers of these atoms in the alkaline-earth oxides and perovskites.

| Reference | | Ba $5s^2, 5p^6, 5d^0, 4f^0$ | Sr $4s^2, 4p^6, 4d^0, 4f^0$ | Ti $3s^2, 3p^6, 3d^2, 4f^0$ | O $2s^2, 2p^4, 3d^0, 4f^0$ |
|---|---|---|---|---|---|
| Core radius (a.u.) | s | 1.75 | 1.50 | 1.30 | 1.15 |
| | p | 2.00 | 1.50 | 1.30 | 1.15 |
| | d | 2.50 | 2.00 | 1.30 | 1.15 |
| | f | 2.50 | 2.00 | 2.00 | 1.50 |

TABLE II: Experimental and theoretical lattice constants ($a$, in Å) for the different compounds involved in our heterostructures. The lattice mismatch, $f$, between a given epilayer and the Si substrate (in % with respect to the substrate lattice constant) is also reported. $d_{A-A}$ (A = Ba or Sr), stands for A-A nearest neighbour distance in AO oxides. Perovskite values refer to the cubic structure.

| System | Experimental | | LDA-DFT | |
|---|---|---|---|---|
| | $a$ (Å) | $f$ (%) | $a$ (Å) | $f$ (%) |
| Si | 5.43 [a] | | 5.389 [b] | |
| BaO | 5.52 [a] | 1.66 | 5.433 | 0.82 |
| | ($d_{Ba-Ba} = 3.90$) | | ($d_{Ba-Ba} = 3.842$) | |
| $BaTiO_3$ | 4.00 [c] | 4.18 | 3.948 | 3.60 |
| Si | 5.43 [a] | | 5.389 [b] | |
| SrO | 5.16 [a] | -4.97 | 5.075 | -5.83 |
| | ($d_{Sr-Sr} = 3.65$) | | ($d_{Sr-Sr} = 3.588$) | |
| $SrTiO_3$ | 3.91 [d] | 1.83 | 3.874 | 0.90 |

[a] N. W. Ashcroft, and N. D. Mermin, Ref. 35.
[b] J. M. Soler *et al.*, Ref. 16.
[c] G. H. Kwei *et al.*, Ref. 36.
[d] T. Mitsui *et al.*, Ref. 37.

and negative when it is expanded. In Table II, we observe that the LDA produces a systematic underestimate of the lattice constant (about 1%). Nevertheless, the correct sequence of lattice mismatch is obtained so that the calculations will reproduce the experimental strain conditions when working at the theoretical lattice constants of the substrate.

Interfaces were simulated using a supercell approximation. The basic unit cell, periodically repeated in space corresponds to the generic $(AO)_n/(AO\text{-}BO_2)_m$ formula, where $n$ and $m$ are respectively the number of AO oxide atomic planes and the number of $ABO_3$ unit cells [7]. For even $n$ and odd $m$ (the only cases studied in this work), this structure possesses two mirror symmetry planes located on the central AO and $BO_2$ layers.

We considered pseudomorphic heterojunctions, so that the lattice constant parallel to the plane of the interface, $a_\parallel$, is assumed to remain the same on both sides of the structure. The choice of $a_\parallel$ allows to treat implicitly the mechanical effect of the substrate, which is not included explicitely in the calculations.

TABLE III: Theoretical values of the elastic constants $c_{11}$ and $c_{12}$ in Mbar.

| | $c_{11}$ | $c_{12}$ | $2(c_{12}/c_{11})$ |
|---|---|---|---|
| BaO | 2.10 | 0.57 | 0.54 |
| $BaTiO_3$ | 3.71 | 1.26 | 0.68 |
| SrO | 2.36 | 0.57 | 0.48 |
| $SrTiO_3$ | 3.93 | 1.17 | 0.59 |

To establish the notation, we will call the plane parallel to the interface the $(x, y)$ plane, whereas the perpendicular direction will be referred to as the $z$ axis.

Under the strain conditions imposed by the Si substrate, the epitaxial layers will minimize the elastic energy by elongation or compression of the lattice constant along $z$, $a_\perp$. To determine its value, strain relaxations of the bulk unit cells of AO and $ABO_3$ were performed under the constraint of fixed $a_\parallel$. Since the lattice misfit between the substrate and the epilayers is small enough to remain in the linear regime, the different values of $a_\perp$ with respect to the in-plane lattice constant can be predicted from the Macroscopic Theory of Elasticity (MTE), and therefore an estimation of the atomic structure of the interface can be done. Following the description of Ref. 38, and for an interface orientation along (001):

$$\begin{aligned} a_{i,\perp} &= \left[1 - D_i \varepsilon_{i,\parallel}\right] a_i \\ \varepsilon_{i,\parallel} &= \frac{a_{i,\parallel}}{a_i} - 1 \\ D_i &= 2\frac{c_{12}^i}{c_{11}^i} \end{aligned} \qquad (1)$$

where $a_i$, $c_{11}^i$ and $c_{12}^i$ stand for, respectively, the equilibrium lattice parameter and the elastic constants of material $i$. Theoretical values of the elastic constants are

TABLE IV: Lattice constant perpendicular to the plane of the interface, $a_\perp$, at different values of the in-plane lattice constant, $a_\parallel$. Results from both, first-principles structural minimizations ($FP$) and macroscopic theory of elasticity ($MTE$) are reported. Units in Å.

| System | $a_\parallel$ | $a_\perp^{MTE}$ | $a_\perp^{FP}$ |
|---|---|---|---|
| | 5.389 | 5.457 | 5.457 |
| BaO | 5.430 | 5.435 | 5.433 |
| | 5.665 | 5.307 | 5.322 |
| | 3.811 | 4.041 | 4.054 |
| $BaTiO_3$ | 3.839 | 4.022 | 4.025 |
| | 4.006 | 3.909 | 3.911 |
| | 5.389 | 4.924 | 4.939 |
| SrO | 5.430 | 4.905 | 4.923 |
| | 5.522 | 4.861 | 4.893 |
| | 3.811 | 3.912 | 3.915 |
| $SrTiO_3$ | 3.839 | 3.895 | 3.893 |
| | 3.904 | 3.856 | 3.857 |

reported in Table III. Bulk structures from the macroscopic theory are in excellent agreement with the first-principles results, as can be drawn from the results in Table IV (relative errors within 1 % for all the cases).

The resulting bulk tetragonal unit cells were used as the building blocks of our supercell. However, as interplanar distances in the region close to the interface are not predicted properly from MTE [39], a full relaxation of the geometry using first principles methods was needed.

For each interface, a *reference* ionic configuration was defined by piling up truncated bulk strained materials. Atomic coordinates were then relaxed until the maximum component of the force on any atom was smaller than 10 meV/Å. The maximum component of the stress tensor along $z$ was smaller than $5 \times 10^{-3}$ eV/Å$^3$ for the Ba-interface and than $7 \times 10^{-3}$ eV/Å$^3$ for the Sr-interface. It has been confirmed that additional relaxation of $a_\perp$ (neglected in this work) does not produce any significant change.

In order to characterize the atomic displacements induced by the relaxation, we define $\delta_z(M_i)$ (respectively $\delta_z(O_i)$) as the displacement of the cation (respectively oxygen) along $z$ at layer $i$, with respect to the initial *reference* configuration. We introduce the displacement of the mean position of each atomic plane as $\beta_i = [\delta_z(M_i) + \delta_z(O_i)]/2$, and the change in the interplanar distance between consecutive planes $i$ and $j$ as $\Delta d_{ij} = \beta_i - \beta_j$. The rumpling parameter of layer $i$ describes the movement of the ions with respect to the mean position of each atomic plane and corresponds to $\eta_i = [\delta_z(M_i) - \delta_z(O_i)]/2$. It is positive when the cation $M_i$ is above the oxygen, and negative otherwise.

Fig. 1 shows a schematic view of the atomic relaxations for both Ba and Sr-interfaces, when the in-plane lattice constant was constrained to the theoretical one of Si. The most important features are: ($i$) a compression of the interplanar distance at the interface layer ; ($ii$) the appearance of an ionic interface dipole, due to the opposite motion of the anion and the cation at the AO-layer closest to the interface – the anion moves towards the AO region whereas the cations displaces inside the $ABO_3$ part –; ($iii$) a monotonic decay of the absolute value of the rumpling parameter as a function of the distance to the AO-interface layer, where the major relaxations are localized, and ($iv$) the oscillatory behaviour of the sign of $\eta_i$ and $\beta_i$ inside the perovskite from layer to layer, as it happens also in $ABO_3$ free-standing slabs[40,41].

The main difference between the Ba and the Sr-heterostuctures is the magnitude of the relaxations at the interface, larger in the last case. All these conclusions are independent of the in-plane lattice constant imposed in the calculation, and show very good agreement with the results obtained using the ABINIT [42] plane-wave pseudopotential code. [43].

## IV. ELECTRONIC STRUCTURE AT THE INTERFACE

In Figure 2, we report the energy band structure along a selected high symmetry line in the first Brillouin zone for the bulk alkaline-earth oxides (ΓX-line) and cubic bulk perovskite structures (ΓR-line). Only bands close to the Fermi level are represented. The valence bands are mainly composed of O $2p$ states that, in the case of the perovskites, show significant hybridizations with Ti $3d$ orbitals.

All the alkaline-earth and perovskite oxides we consider are insulators (experimental gaps above 3 eV). Within the cubic symmetry (in the absence of strains) and neglecting spin-orbit couplings, the computed band gap for both $BaTiO_3$ and $SrTiO_3$ is indirect ($R \rightarrow \Gamma$). The top-most valence and the bottom-most conduction bands are three times degenerated at these high symmetry points. Under the same conditions, the gap is also indirect in SrO, with three degenerated upper most valence bands at Γ and a single lowest conduction band at $X$, whereas BaO exhibits a direct gap, between single bands at $X$.

In Table V we report experimental and theoretical bands gaps (within LDA) for all the materials involved in our study. We see that, due to the well known DFT "band gap problem", the theoretical values are understimated by about 50 % in each case. Nevertheless, it is usually accepted that this error can be roughly compensated by an appropriate shift of the conduction bands which should not affect the conclusions of the character of the gap reported in this Section.

A uniaxial strain along (001) lowers the symmetry of the perovskites from Pm3m to P4mm. This translates into a splitting of the top of the valence bands into a singlet and a doublet. The singlet is above (below) for

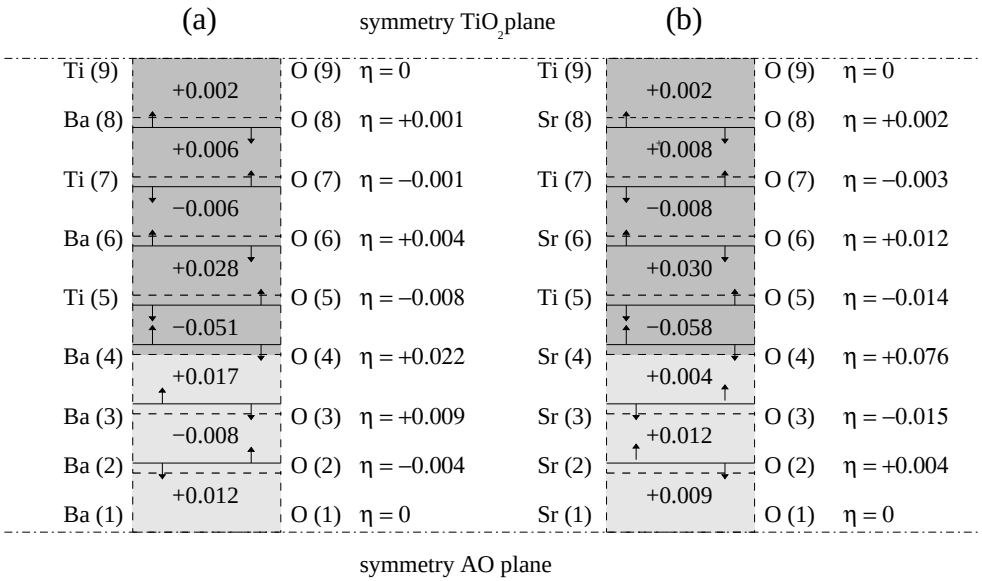


FIG. 1: Schematic view of the atomic relaxation for the bottom half of $BaO/BaTiO_3$ (panel a), and $SrO/SrTiO_3$ (panel b) supercells. Dashed lines correspond to the *reference* positions of the atomic planes, and the full lines are the mean position in the relaxed structure. Changes in the interplanar distance are written in Å. The atoms (A or Ti, depending on the layer, at the left and O at the right) move in the direction indicated by the arrow. The rumpling parameter, $\eta$, is expressed in Å. The size of the heterostructure corresponds to $n$=6, $m$=5.

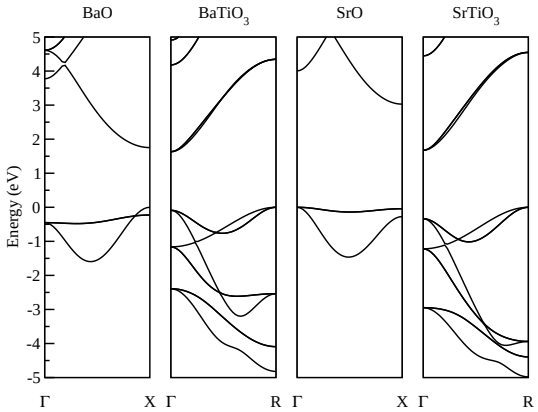


FIG. 2: Bulk band structures of cubic BaO, $BaTiO_3$, SrO, and $SrTiO_3$ at the theoretical lattice constant. The zero of energy has been asigned to the top of the valence band in each case. Only the bands closed to the gap are plotted.

a compressive (tensile) strain. For the alkaline-earth oxides, the symmetry reduces from $Fm\overline{3}m$ to I4/mmm. The top of the valence band of SrO is therefore split but, in this case, the doublet is above (below) the singlet for a compressive (tensile) strain. Spin-orbit couplings (not considered in this work) might introduce further splittings.

Fig. 3 shows the Projected Density Of States (PDOS) on the different atoms (sum of the projections of the DOS on all the atomic orbitals of the given atom) as a function of the depth of the layer inside the material for the $BaO/BaTiO_3$ and $SrO/SrTiO_3$ interfaces. The main conclusions that can be extracted are as follows: (*i*) the absence of any interface induced gap states clearly demonstrates the semiconductor character of the heterostructures; (*ii*) the features of the PDOS on the alkaline-earth and the O atom at the interface layer (labelled as 4) are much closer to the ones displayed in bulk-$ABO_3$ than in bulk-AO, showing a dominant $ABO_3$ character of the interface; (*iii*) the PDOS converges very quickly to the bulk properties and many of the bulk features can be recovered even at the atomic layers closest to the interface; (*iv*) atomic relaxations have small effects on the shape of the PDOS, as can be seen comparing the solid and dotted curves in the figure. Only a shift in the SrO layers towards the zero energy (chosen as the top of the valence

TABLE V: Theoretical ($E_{gap}^{theo}$) and experimental ($E_{gap}^{expt}$) band gaps in eV for the materials involved in our simulations. The theoretical value, within LDA, has been calculated at the theoretical lattice constant.

| | BaO | $BaTiO_3$ | SrO | $SrTiO_3$ |
|---|---|---|---|---|
| $E_{gap}^{theo}$ | 1.75 | 1.63 | 3.03 | 1.67 |
| $E_{gap}^{expt}$ | 4.8 [a] | 3.2 [b] | 5.7 [a] | 3.3 [c] |

[a] W. H. Strehlow, and E. L. Cook, Ref. 44.
[b] S. H. Wemple, Ref. 45.
[c] R. A. McKee, F. J. Walker, and M. F. Chisholm, Ref. 7.

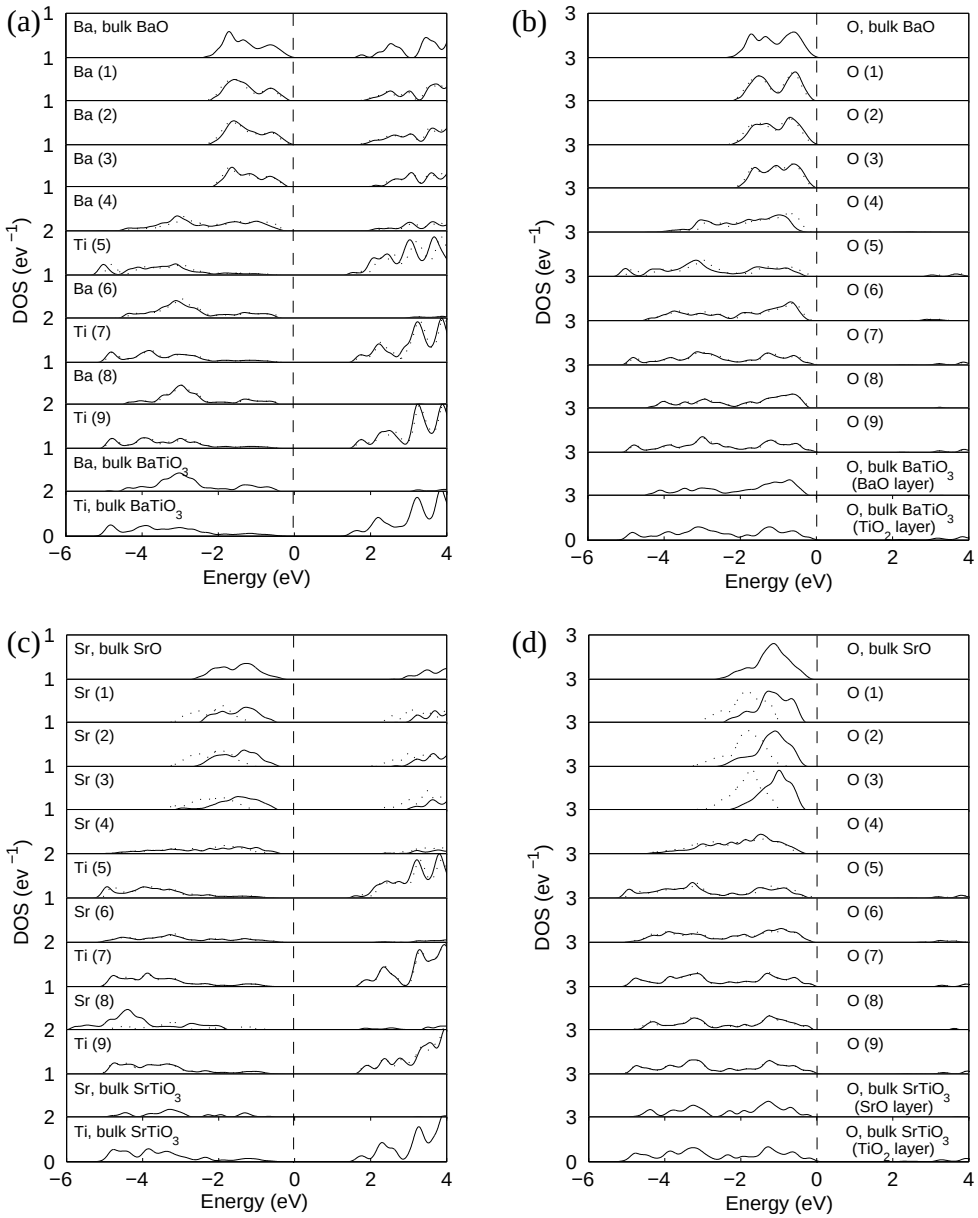


FIG. 3: Projected Density Of States on all the atoms as a function of the distance to the interface for the $BaO/BaTiO_3$ (panels a and b) and $SrO/SrTiO_3$ (panels c and d) heterostructures. Full lines represent the projection for the relaxed geometry and dotted lines for unrelaxed coordinates. Atomic layers are identified as in Fig. 1. Projected Density Of States of bulk AO and $ABO_3$ are also plotted for comparison. All the energies have been rigidly displaced in order to align the top of the valence band (vertical line) with zero. The imposed $a_{\parallel}$ was set up to the theoretical one of Si (5.389 Å).

band in each case) is noticeable. This effect is a direct consequence of the relaxation-induced interface dipole discussed in Section III. The different magnitude of the dipole between the Ba and Sr-interfaces explains why the shift is almost negligeable in the Ba-heterostructure.

## V. BAND OFFSET

One of the most important physical quantities that characterize the interface between semiconductors or insulators is the band offset, i. e., the relative position of the energy levels on both sides of the interface. The valence-band offset, VBO (respectively conduction-band offset, CBO) is defined as the difference between the positions of the top of the valence bands (respectively the

bottom of the conduction bands) of the two materials. These band discontinuities play a fundamental role in calculating the transport properties through heterojunction devices.

The determination of these offsets from first-principles cannot be achieved from a direct comparison of the corresponding band edges in the two compounds as obtained from two independent bulk band-structure calculations. The reason is the lack of an intrinsic energy scale to refer all the energies: in a first-principles simulation, the hamiltonian eigenvalues are referred to an average of the electrostatic potential that is ill-defined for infinite systems[46] (it is only defined to within an arbitrary constant). Consequently, together with the eigenvalue difference, we must consider the lineup of this average between the two materials. This potential shift depends on the dipole induced by the electronic charge transferred from one part of the interface to the other after the interfacial hybridization (the electronic charge density of each system will decay into the other in an, in principle, unknown way). The transfer of charge depends not only on the materials that constitute the interface, but also on the particular orientation, so the lineup can only be obtained from a self-consistent calculation on a supercell including both materials.

Therefore, from the theoretical point of view, the band offsets (BO) are usually split into two terms [47,48]:

$$\mathrm{BO} \;=\; \Delta E_{v,c} + \Delta V \tag{2}$$

The first contribution, $\Delta E_v$ (resp. $\Delta E_c$), is referred to as the *band-structure term*. It is defined as the difference between the top (resp. bottom) of the valence (resp. conduction) bands as obtained from two independent standard bulk band-structure calculations at the same strained geometries as in the supercell construction. Within LDA, only a first estimate of the band-structure term can be obtained, $\Delta E_{v,c}^{LDA}$. To get more accurate results, a correction dealing with many-body effects in the quasiparticle spectra should be added:

$$\Delta E_{v,c} = \Delta E_{v,c}^{LDA} + \Delta E_{v,c}^{corr} \tag{3}$$

Self-energies corrections are often obtained within the GW approximation[49]. They strongly modify the description of the conduction bands, and tend to solve the "band gap problem" mentioned in Section IV. Even the valence band energies might be subject of certain errors, specially in oxides[50]. Unfortunately, no accurate GW data are currently available for AO and $ABO_3$ compounds. Only model GW calculations have been performed recently for SrO and $SrTiO_3$ and with limited success[51]. To overcome the problem, we make the approximation that the errors in the valence bands are smaller than those for the conduction bands and of the same order of magnitude for the two compounds taking part in the heterostructures so that they tend to cancel each other ($\Delta E_v^{corr} = 0$). Knowing the relative position of the valence bands, we simply add the experimental band gaps (see Table V) to obtain the discontinuities for the conduction bands ($\Delta E_c = \Delta E_v^{LDA} + \Delta E_{gap}^{expt}$).

The second term, $\Delta V$, is the *lineup of the average of the electrostatic potential* through the heterojunction. This macroscopic quantity summarizes all the intrinsic interface effects, such as the chemical composition, structural details and orientation. To obtain it, we start from the total (ionic plus electronic) microscopic electrostatic Hartree potential, output of the self-consistent supercell calculation (in this Section we will define the zero-energy level as the average of this potential in the unit cell [52]). Then, we apply the double-macroscopic average[47,48,53] technique. It consists of performing first the average of the electrostatic potential over planes parallel to the interface, and then averaging the obtained quasiperiodic one-dimensional function with two step-like filter functions whose lenghts, $l_1$ and $l_2$, are determined by the periodicity of the constituents. Here $l_1$ and $l_2$ have been set up to the distance between equivalent AO and $TiO_2$ planes in the alkaline-earth oxide and in the perovskite respectively. A full description of the method to the $AO/ABO_3$ heterostructures can be found in Ref. 54. The resulting profile of the macroscopic potential is flat on both sides far enough from the interface (*bulk-like regions*). $\Delta V$ is defined as the difference between these two plateau values (see Fig. 4). The lineup should be independent of the length used in the filter functions. However we have checked how doubling the size of the step-like functions introduce a numerical uncertainty in $\Delta V$ of the order of 30 meV. This is the main source of inaccuracy in our calculations of the band offsets.

It is worth noticing that neither $\Delta E_v$ nor $\Delta V$ have any physical meaning by their own, being pseudopotential dependent numbers. Only the sum of both is physically significant and quite independent of the choice of the pseudopotential [48].

### A. First principles results

Fig. 4 shows a schematic representation of the band structure discontinuities for the $BaO/BaTiO_3$ and $SrO/SrTiO_3$ heterostructures, both of them calculated fixing the in-plane lattice constant at the theoretical one of Si. Band splittings steming from strain are taken into account in the figure. We use the same sign convention as Van de Walle and Martin in Ref. 55: a positive value of the band offset for the discontinuity at a junction A/B corresponds to an upward step in going from A to B.

From the figure, we conclude that Ba-interface is type-II, with both the valence and conduction bands of $BaTiO_3$ falling in energy below the corresponding ones of BaO. Within the accuracy of our calculations, BaO and $BaTiO_3$ topmost valence bands are almost aligned (an offset of only -0.06 eV is predicted), so the barrier in the conduction bands is mainly due to the difference in

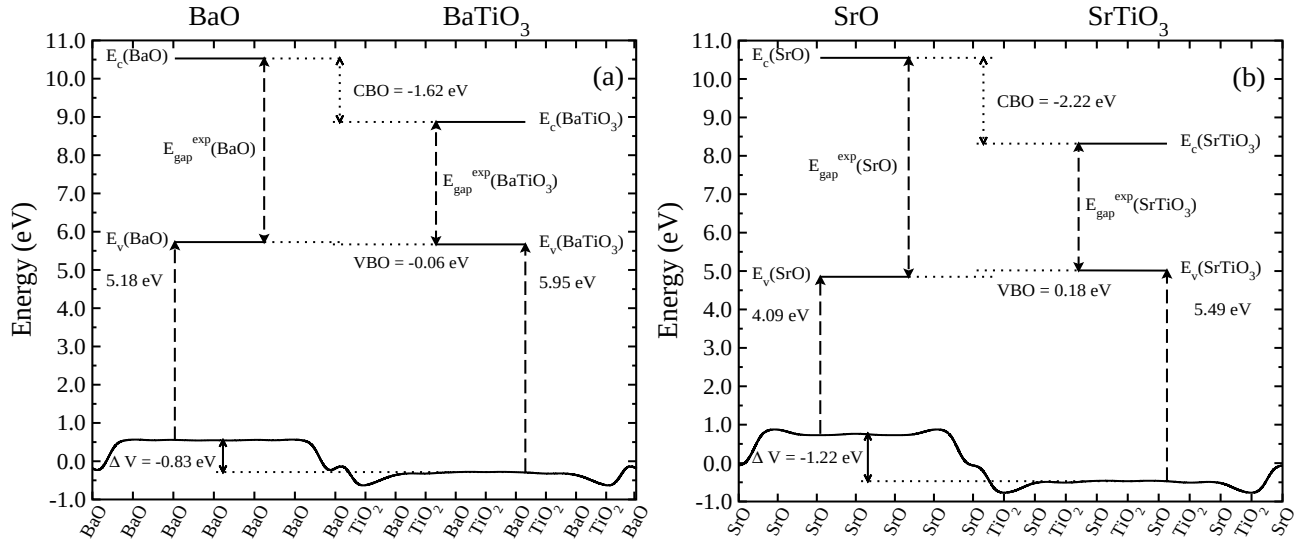


FIG. 4: Schematic representation of the valence-band offset (VBO) and the conduction-band offset (CBO) for $BaO/BaTiO_3$ (panel a), and $SrO/SrTiO_3$ interface (panel b). $E_v$, $E_c$, and $E_{gap}^{exp}$ stand for the top of the valence band, the bottom of the conduction band and the experimental band gap respectively. Values for $E_v$, measured with respect to the average of the electrostatic potential in each material, are indicated. The solid curve represents the profile of the macroscopic average of the total electrostatic potential across the interface. $\Delta V$ stands for the resulting lineup. The in-plane lattice constant was set up to the theoretical one of Si (5.389 Å). The size of the supercell corresponds to $n = 6$ and $m = 5$.

the band gaps of both materials and, inferred from the experimental values, amounts to -1.62 eV.

Sr-interface is type-I, meaning that the band gap of $SrTiO_3$ lies completely inside the gap of SrO. An upward step of +0.18 eV for the valence bands is theoretically expected, which implies a CBO of -2.22 eV.

A rough estimate of the valence band offset was already accessible [56] by identifying in Fig. 3 the position of the top of the valence band in the PDOS for the O atom at both symmetry planes, in the bulk-like regions of the materials that constitute the interface (numbered as 1 for AO and 9 for $ABO_3$). The values deduced from the figure are -0.09 eV for the Ba-interface (BaO above) and +0.28 eV for the Sr-interface ($SrTiO_3$ above), close to those obtained using the macroscopic average technique. However these numbers must be taken with care[48]: this method to compute band offsets requires calculations with a higher number of special $\vec{k}$-points than those needed to converge the charge density or the potential lineup.

It is important to note here the *crucial* role played by the atomic relaxations at these polar interfaces. As was pointed out in section III, after the relaxation process an extra dipole appears at the junction that modifies the electrostatic lineup accross the interface [57] and, consequently, the band offsets :

$$\delta(\Delta V) = \frac{4\pi}{a_\parallel^2} \sum_{\kappa\alpha} \frac{Z^{*(T)}_{\kappa,\alpha z}}{\epsilon_\infty} \Delta u_{\kappa\alpha} \qquad (4)$$

where $\delta(\Delta V)$ is the change in the electrostatic lineup along $z$-direction due to the atomic displacements, $Z^{*(T)}_{\kappa,\alpha\beta}$ is the Born effective tensor of atom $\kappa$, $\Delta u_{\kappa\alpha}$ its displacement along cartesian direction $\alpha$ during the relaxation and $\epsilon_\infty$ the optical dielectric constant. Looking at the magnitude of the atomic displacements, it is reasonable that the change should be more remarkable for the Sr-interface than for the Ba one. From our *ab-initio* calculations, and for the same supercell used to get results in Fig. 4, we observe a change in $\Delta V$ of -0.67 eV for the Sr-interface (from 1.16 eV for the unrelaxed geometry to 0.49 eV after the relaxation), whereas in the Ba-interface the deviation amounts to -0.11 eV (from 0.44 eV to 0.33 eV). This emphasizes the importance of performing accurate first-principles atomic relaxations for correct predictions of the barriers.

To what extent do these discontinuities change with

TABLE VI: Valence-band offsets (VBO) for $BaO/BaTiO_3$ and $SrO/SrTiO_3$ interfaces. Values are reported at different in-plane lattice constants, $a_\parallel$. $\Delta E_v$ and $\Delta V$ stand for, respectively, the band structure term and the line up of the electrostatic potential contributions to VBO. The size of the heterostructures corresponds to $n = 6$, $m = 5$.

| | $BaO/BaTiO_3$ | | | | $SrO/SrTiO_3$ | | |
|---|---|---|---|---|---|---|---|
| $a_\parallel$ (Å) | 5.389 | 5.430 | 5.583 | 5.665 | 5.389 | 5.430 | 5.522 |
| $\Delta V$ | -0.834 | -0.833 | -0.746 | -0.755 | -1.217 | -1.190 | -1.128 |
| $\Delta E_v$ | 0.772 | 0.807 | 0.600 | 0.560 | 1.401 | 1.340 | 1.209 |
| VBO | -0.062 | -0.026 | -0.146 | -0.195 | 0.184 | 0.150 | 0.081 |

the in-plane lattice constant? This is an important question because a dependence with strain would allow us to tune the band offsets (for example, replacing the Si substrate by Ge[7] in order to impose a different lattice parameter throughout the interface) depending on the required values for a given device. In order to check this point, we have carried out calculations at different in-plane lattice constants. In Table VI and Fig. 5 we summarize the results for both, Ba and Sr-heterostructures. In both cases a variation by about 0.1 eV in VBO with the in-plane lattice constant is observed, mainly due to the band-structure term (consequence of the strain-induced splittings of the top valence-band manifold), as it happens for other lattice-mismatched, isovalent, common anion interfaces [58]. The change is almost linear, and tends to lower the energy of the valence bands of the $ABO_3$ perovskite with respect to the AO alkaline-earth oxide.

The band-structure term displays a linear behaviour with strain for the Sr-interface (see Fig. 5-panel a). The anomalous behaviour of $\Delta E_v$ for the Ba-interface is due to a modification in the character of the top of the valence band of BaO under strain. It changes from $X$ when BaO is compressed to $Z$ when it is expanded. This transformation occurs for a lattice constant around 5.43 Å (theoretical lattice parameter of BaO). In Fig. 5(a) we plot the difference between the top of the valence band of $BaTiO_3$ and the highest occupied state at $X$ and $Z$ of BaO. The crossing point is clearly identified in the figure. No extra changes in the linear beaviour of $\Delta E_v$ are expected for longer lattice constants.

The almost-linear change in the lineup term can be explained according to an analytic scaling law proposed in Ref. 59. Once $\Delta V$ is known for a reference configuration with an in-plane lattice constant $a_{\parallel}$, then, supposing an uniform strain throughout the structure, $\Delta V'$ for any other strained configuration $a_{\parallel}^{'}$ can be extrapolated from:

$$\Delta V^{'} \simeq \frac{1}{\left(1+\varepsilon_{\parallel}^{2}\right)} \Delta V \qquad (5)$$

where $\varepsilon_{\parallel} = (a_{\parallel}^{'}/a_{\parallel} - 1)$. Fig. 5(b) shows a comparison of the first-principles and extrapolated values, where the heterostructure at the in-plane lattice constant of Si has been chosen as the reference configuration. Results are in good agreement within the numerical accuracy of the *ab-initio* results.

In summary, the VBO varies almost linearly for a large range of in-plane strains. The only deviation is observed for $BaO/BaTiO_3$ and is explained by a change of character of the BaO gap under compression.

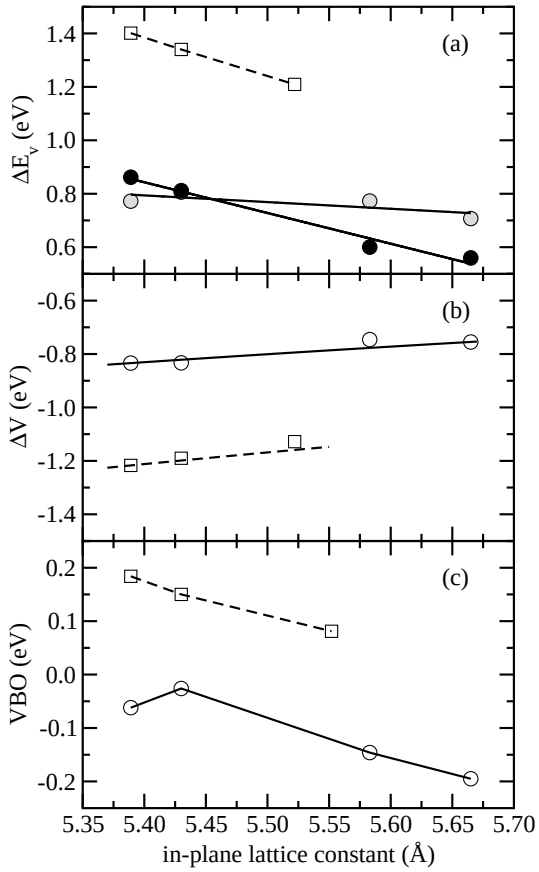


FIG. 5: Dependence with in-plane strain of the valence-band offset (VBO), and of its decomposition into the band-structure ($\Delta E_v$), and lineup ($\Delta V$) terms. Squares and circles represent, respectively, the first-principles results for the $SrO/SrTiO_3$ and $BaO/BaTiO_3$ interfaces. In panel (a), grey-filled (respectively black-filled) circles stand for the diffrence between the top of the valence band of $BaTiO_3$ and the highest occupied state at X (respectively Z) point in BaO. Lines in panels (a) and (c) (dashed for Sr and full for the Ba-interface), are a guide to the eye. Lines in panel (b) represent the results of the anayltic scaling law proposed in Ref. 59.

## VI. INTERFACE WITH SI

As it was pointed out in the Introduction, $AO/ABO_3$ interface is only a part of the gate stack of technological interest for the semiconductor industry. AO acts as a buffer layer between the Si substrate and the high-$\kappa$ perovskite. The whole heterostructure epitaxially grown following the McKee-Walker process [8] is made of $Si/ASi_2/AO/ABO_3$ [6]. As it will be emphasized in this Section, the role of the buffer layer is not only the passivation of the Si substrate, but also the efficient tuning of the offsets between the perovskite and the channel.

Combining our results with various data available in the literature, we can estimate the band discontinuities along the whole heterostructures of technological interest as summarized in Fig. 6. Previous theoretical calculations of the band offsets between the alkaline-earth oxide AO and Si have been reported recently ($Si/BaO$[61], $Si/SrO$[60]. In addition, we can find in the literature theoretical estimations for the Schottky barriers between perovskites and prototypical metallic electrodes ($SrTiO_3$/Pt

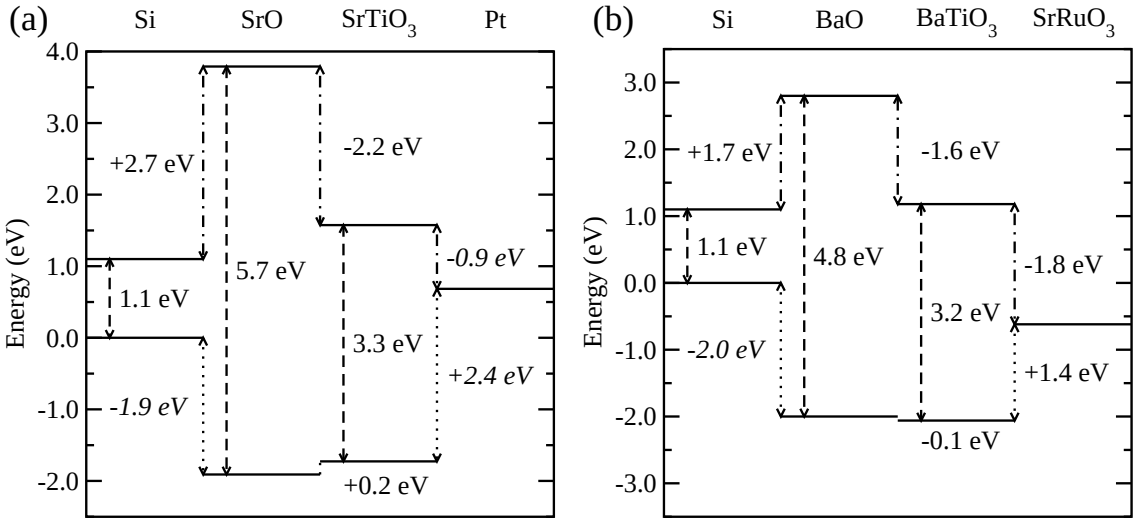


FIG. 6: Estimation of the valence (dotted lines) and conduction (dot-dashed lines) band offsets for the whole heterostructures $Si/SrO/SrTiO_3/Pt$ (panel a), and $Si/BaO/BaTiO_3/SrRuO_3$ (panel b). Dashed lines represent the experimental band gaps. Theoretical value for the VBO between Si and AO (in italic) has been taken from Ref. 60 for the Sr interface, and from Ref. 61 for Ba-interface. Theoretical Schottky-barriers between $SrTiO_3$ and Pt (also in italic) have been taken from Ref. 11.

[11], or $BaTiO_3/SrRuO_3$[62]).

We must notice that, altough most of the previous works (except Ref. 11) have been done using the same basic approaches (DFT, pseudopotentials, $\vec{k}$-point samplings, supercells, etc), they differ in the details of the calculations (for example, they have been carried out at different in-plane lattice constant, and the size of the supercells, or the parameters used to generate the pseudopotentials might change from one to the other). So, only a rough estimate of the barriers can be deduced from the comparison and any quantitative conclusion is beyond the scope of this Section.

Within LDA, plus GW corrections, Boungiorno-Nardelli *et al.* [60] investigated the structural and electronic properties of the $Si/SrSi_2/SrO$ interface. They predicted a VBO between Si and SrO of -1.91 eV for the most stable interface configuration. Using the experimental gaps to locate the conduction bands, it translates in a CBO of 2.69 eV. The Schottky barrier $\phi_n$ (difference between the Fermi level and the bottom of the conduction band) between $SrTiO_3$ and Pt has been evaluated [11] to -0.89 eV, which implies a barrier height $\phi_p$ (difference between the Fermi level and the top of the valence band) of 2.41 eV. These results are summarized in the first panel of Figure 6.

Through first-principles gradient-density-functional calculations Gulleri *et al.* [61] focused on the structure, energetic and band offsets of the Si/BaO interface. For the favoured geometry, they obtained a VBO of -2.0 eV. Some of us evaluated the Schottky barriers between $BaTiO_3$ and $SrRuO_3$ (a typical metallic electrode in ferroelectric devices [63]) to be equal to $\phi_p = +1.44$ eV and $\phi_n$ = -1.76 eV. These results are summarized in the second panel of Figure 6.

For both stacks, we can clearly see how the problem of the large carrier injection (expected for the perovskite in direct contact with Si[11]) is overcome by the use of the AO layer. The electrostatic barriers for both the electrons and holes, between the gate electrode and the channel are large enough to prevent carrier injections and to push the use of $ABO_3$ perovskites to a prominent position to replace silica as the gate dielectric oxide in MOSFETs.

## VII. CONCLUSIONS

We have studied structural and electronic properties of $BaO/BaTiO_3$ and $SrO/SrTiO_3$ interfaces from first-principles. Atomic relaxations have been performed. Interface dipoles, due to the opposite motion of the anion and cation atoms at the interface, appear for both heterostructures. No interface electronic states are induced in the band gap. The character of the AO layer at the interface is mainly perovskite-like. Under the experimental strain conditions, the valence bands of BaO and $BaTiO_3$ are almost aligned (within the accuracy of our calculations), whereas a slightly larger barrier is predicted for $SrO/SrTiO_3$. Interface dipoles, induced by atomic relaxations, have a strong effect on the band alignments at the interface. A nearly linear variation of the VBO with in-plane strain is observed.

Gathering together our results and various data available in the literature, we make a guess for the band alignment of whole $Si/SrO/SrTiO_3/Pt$ and $Si/BaO/BaTiO_3/SrRuO_3$ structures. In both cases large enough electrostatic barriers for electrons and holes between the gate electrode and the channel are estimated, preventing the injection of carriers and suggesting that

both perovskites compounds are promising candidates to replace silica in MOSFETs. Our results should be confirmed by more accurate calculations for the whole heterostructure.

## VIII. ACKNOWLEDGMENTS

The authors are indebted with Maria Peressi, Luciano Colombo, Rodney McKee, Marco Buongiorno-Nardelli, Hermann Kohlstedt, Darrel Schlom, Alex Demkov, and Jun Wang for useful discussions. Motorola PSRL supported the initial stages of this work. This work was supported by the Volkswagen-Stiftung (www.volkswagenstiftung.de) within the program "Complex Materials: Cooperative Projects of the Natural, Engineering, and Biosciences" with the title: "Nanosized ferroelectric Hybrids" under project number I/77 737. Three of us (J. J., M. Z., and Ph. G.) acknowledge support from FNRS-Belgium (grants 9.4539.00 and 2.4562.03) and the Université de Liège (Impulsion grant). J. J. and P. O. acknowledge finantial support from the Fundación Ramón Areces and Spanish MCyT grant BFM2000-1312. Calculations have been performed on the NIC computer at the Université de Liège, and on computational resources from CESCA and CEPBA.

[1] An exhaustive review of this topic can be found in the MRS Bulletin, **27**, 186-229 (2002), R. M. Wallace and G. Wilk, Guest Editors.
[2] International Technology Roadmap for Semiconductors, Semiconductors Association, San Jose, 2002. Home page, http://public.itrs.net (accessed January 2002).
[3] G. Wilk and R. M. Wallace, J. Appl. Phys. **89**, 5243 (2001).
[4] D. G. Schlom, C. A. Billman, J. H. Haeni, J. Lettieri, P. H. Tan, R. R. M. Held, S. Völk, and K. J. Hubbard, Appl. Phys. A (in press) (2002).
[5] A. A. Demkov, Phys. Stat. Sol. (b) **226**, 57 (2001).
[6] R. A. McKee, F. J. Walker, and M. F. Chisholm, Phys. Rev. Lett. **81**, 3014 (1998).
[7] R. A. McKee, F. J. Walker, and M. F. Chisholm, Science **293**, 468 (2001).
[8] R. A. McKee, and F. J. Walker, US Patent No. 5,830,270 (November 3, 1998).
[9] R. A. McKee, F. J. Walker, J. R. Conner, E. D. Specht, and D. E. Zelmon, Appl. Phys. Lett. **59**, 782 (1991).
[10] K. Eisenbeiser, J. M. Finder, Z. Yu, J. Radmani, J. A. Curless, J. A. Hallmark, R. Droopard, W. J. Ooms, L. Salem, S. Bradshaw, et al., Appl. Phys. Lett. **76**, 1324 (2000).
[11] J. Robertson and C. W. Chen, Appl. Phys. Lett. **74**, 1168 (1999).
[12] J. Tersoff, Phys. Rev. B **30**, 4874 (1984).
[13] S. A. Chambers, Y. Liang, Z. Yu, R. Droopad, and J. Radmani, J. Vac. Sci. Technol. A **19**, 934 (2001).
[14] P. Hohenberg and W. Kohn, Phys. Rev. **136**, B864 (1964).
[15] W. Kohn and L. J. Sham, Phys. Rev. **140**, A1133 (1965).
[16] J. M. Soler, E. Artacho, J. D. Gale, A. García, J. Junquera, P. Ordejón, and D. Sánchez-Portal, J. Phys: Condens. Matter **14**, 2745 (2002).
[17] D. Sánchez-Portal, E. Artacho, P. Ordejón, and J. M. Soler, Int. J. Quantum Chem. **65**, 453 (1997).
[18] P. Ordejón, E. Artacho, and J. M. Soler, Phys. Rev. B **53**, R10441 (1996).
[19] J. P. Perdew and A. Zunger, Phys. Rev. B **23**, 5048 (1981).
[20] D. M. Ceperley and B. J. Alder, Phys. Rev. Lett. **45**, 566 (1981).
[21] L. Kleinman and D. J. Bylander, Phys. Rev. Lett. **48**, 1425 (1982).
[22] N. Troullier and J. L. Martins, Phys. Rev. B. **43**, 1993 (1991).
[23] O. F. Sankey and D. J. Niklewsky, Phys. Rev. B **40**, 3979 (1989).
[24] E. Artacho, D. Sánchez-Portal, P. Ordejón, A. García, and J. M. Soler, Phys. Stat. Sol. (b) **215**, 809 (1999).
[25] J. Junquera, O. Paz, D. Sánchez-Portal, and E. Artacho, Phys. Rev. B **64**, 235111 (2001).
[26] Values for the parameters can be obtained upon request.
[27] H. J. Monkhorst and J. D. Pack, Phys. Rev. B **13**, 5188 (1976).
[28] J. Moreno and J. Soler, Phys. Rev. B **45**, 13891 (1992).
[29] R. D. King-Smith and D. Vanderbilt, Phys. Rev. B **49**, 5828 (1994).
[30] P. Ordejón, E. Artacho, R. Cachau, J. Gale, A. García, J. Junquera, J. Kohanoff, M. Machado, D. Sánchez-Portal, J. Soler, et al., Mat. Res. Soc. Symp. Proc. **677**, AA9.6.1 (2001).
[31] Ph. Ghosez, E. Cockayne, U. V. Waghmare, and K. M. Rabe, Phys. Rev. B **60**, 836 (1999).
[32] Ph. Ghosez, X. Gonze, P. Lambin, and J.-P. Michenaud, Phys. Rev. B **51**, 6765 (1995).
[33] Z. Zhong, R. D. King-Smith, and D. Vanderbilt, Phys. Rev. Lett. **72**, 3618 (1994).
[34] R. E. Cohen and H. Krakauer, Phys. Rev. B **42**, 6416 (1990).
[35] N. W. Ashcroft and N. D. Mermin, *Solid State Physics* (Saunders College Publishing, Philadelphia, 1976).
[36] G. H. Kwei, A. C. Lawson, S. J. L. Billingue, and S. W. Cheong, J. Phys. Chem. **97**, 2368 (1993).
[37] *Numerical Data and Functional Relations in Science and Technology-Crystal and Solid State Physics*, edited by T. Mitsui and S. Nouma, Landolt-Börnstein, New Series, Group III, Vol. 16, Pt. a (Springer, Berlin, 1982).
[38] C. G. Van de Walle and R. M. Martin, Phys. Rev. B **34**, 5621 (1986).
[39] M. Peressi, L. Colombo, A. Baldereschi, R. Resta, and S. Baroni, Phys. Rev. B **48**, 12047 (1993).
[40] J. Padilla and D. Vanderbilt, Phys. Rev. B **56**, 1625 (1997).
[41] C. Cheng, K. Kunc, and M. H. Lee, Phys. Rev. B **62**, 10409 (2000).
[42] X. Gonze, J. -M. Beuken, R. Caracas, F. Detraux, M. Fuchs, G. -M. Rignanese, L. Sindic, M. Verstraete, G. Zerah, F. Jollet, et al., Comp. Mat. Sci. **25**, 478 (2002).
[43] M. Zimmer, J. Junquera, and Ph. Ghosez, AIP Conf. Proc. **626**, 232 (2002).
[44] W. H. Strewlow and E. L. Cook, J. Phys. Chem., Ref. Data **2**, 163 (1973).
[45] S. H. Wemple, Phys. Rev. B **2**, 2679 (1970).

[46] L. Kleinman, Phys. Rev. B **24**, 7412 (1981).
[47] L. Colombo, R. Resta, and S. Baroni, Phys. Rev. B **44**, 5572 (1991).
[48] M. Peressi, N. Binggeli, and A. Baldereschi, J. Phys. D: Appl. Phys. **31**, 1273 (1998).
[49] M. S. Hybertsen and S. G. Louie, Phys. Rev. B **34**, 5390 (1986).
[50] B. Kralik, E. K. Chang, and S. G. Louie, Phys. Rev. B **57**, 7027 (1998).
[51] G. Capellini, S. Bouette-Russo, B. Amadon, C. Noguera, and F. Finocci, J. Phys. Condens. Matter **12**, 3671 (2000).
[52] As it is usual within first-principles codes, in this paper we define the zero-energy level as the $\vec{G} = \vec{0}$ Fourier-component (i. e., the mean value over the unit cell) of the total (ionic plus electronic) electrostatic potential, $V^H(\vec{r})$. This is not the case within the SIESTA method, where the reference is assigned to the average of $\delta V^H(\vec{r})$, the electrostatic potential generated by the deformation charge density, $\delta\rho(\vec{r})$, defined [16] as the difference between the self-consistent electronic charge density and the sum of atomic densities, $\rho^{atom} = \sum_I \rho_I^{atom}$. The difference between $V^H(\vec{r})$ and $\delta V^H(\vec{r})$ (the so-called the Neutral Atom potential in Ref. 16) is a short-range local component, (therefore a bulk quantity not dependent in the details of the interface). In this work, to remain compatible with our choice for the reference, its lineup is included in the band-structure term.
[53] A. Baldereschi, S. Baroni, and R. Resta, Phys. Rev. Lett. **61**, 734 (1988).
[54] J. Junquera and P. Ordejón, NATO Science Series II *Atomistic Aspects in Epitaxial Growth* (Ed. Kluwer Academic Publishers) **65**, 561 (2002).
[55] C. G. Van de Walle and R. M. Martin, Phys. Rev. B **35**, 8154 (1987).
[56] F. Rao, M. Kim, A. J. Freeman, S. Tang, and M. Anthony, Phys. Rev. B **55**, 13953 (1997).
[57] R. Martin and K. Kunc, Phys. Rev. B **24**, 2081 (1981).
[58] M. Di Ventra, M. Peressi, and A. Baldereschi, Phys. Rev. B **54**, 5691 (1996).
[59] M. Di Ventra, M. Peressi, and A. Baldereschi, J. Vac. Sci. Technol. B **14**, 2936 (1996).
[60] M. Buongiorno-Nardelli, W. A. Shelton, and G. Malcom Stocks, Bulletin of The American Physical Society **47**, 892 (2002).
[61] G. Gulleri, and V. Fiorentini, private communication.
[62] J. Junquera, and Ph. Ghosez, unpublished.
[63] C. B. Eom, R. J. Cava, R. M. Fleming, J. M. Phillips, R. B. van Dover, J. H. Marshall, J. W. P. Hsu, J. J. Krajewski, and W. F. Peck Jr., Science **258**, 1766 (1992).